Spectroscopic characterization of the X(10+) and A(30+) states of CdNe, CdAr, CdKr, and CdXe

Agust Kvaran, David J. Funk, Andrzej Kowalski, and W. H. Breckenridge

Citation: J. Chem. Phys. **89**, 6069 (1988); doi: 10.1063/1.455422
View online: http://dx.doi.org/10.1063/1.455422
View Table of Contents: http://jcp.aip.org/resource/1/JCPSA6/v89/i10
Published by the American Institute of Physics.

Spectroscopic characterization of the $X(^1\Sigma^+)$ and $A(^3\Sigma^+)$ states of CdNe, CdAr, CdKr, and CdXe

Agust Kvaran,[a] David J. Funk, Andrzej Kowalski,[b] and W. H. Breckenridge
Department of Chemistry, University of Utah, Salt Lake City, Utah 84112

(Received 1 July 1988; accepted 10 August 1988)

We report the spectroscopic characterization of the $X(^1\Sigma^+)$ and $A(^3\Sigma^+)$ states of CdNe, CdAr, CdKr, and CdXe. The van der Waals molecules were created in a free jet supersonic expansion and studied by low and high resolution laser-induced fluorescence. CdAr was also studied by dispersed fluorescence. A method of analyzing rotationally structured vibrational bands of overlapping isotopic spectral contributions is discussed. Spectroscopic parameters are obtained from computer simulations of CdNe and CdAr spectra and from analysis of vibrational isotope splittings for CdKr and CdXe. CdNe: $r_e''(X \text{ state}) = 4.26 \pm 0.05$ Å, $r_e'(A \text{ state}) = 3.62 \pm 0.05$ Å, $D_e'(A \text{ state}) = 77\ \text{cm}^{-1}$; CdAr: $r_e''(X) = 4.33 \pm 0.04$ Å, $r_e'(A) = 3.45 \pm 0.03$ Å, $D_e'(A) = 325\ \text{cm}^{-1}$; CdKr: $D_e'(A) = 513\ \text{cm}^{-1}$ and CdXe: $D_e'(A) = 1086\ \text{cm}^{-1}$.

INTRODUCTION

Determination of the potential curves for the interactions of ground and excited states of metal atoms with the inert gases is not only important in understanding van der Waals bonding, but is also useful in interpreting dynamical processes such as electronic energy transfer,[1–6] resonance radiation collisional redistribution,[7] elastic and inelastic scattering,[8,9] and van der Waals complex excitation "half-collision" experiments.[6,10–12] One of the most successful techniques for accurately measuring such potential curves has been the use of laser spectroscopy to characterize M·Rg (M = metal, Rg = rare gas) van der Waals complexes created and cooled in supersonic jet expansions.[6,12–22] Such studies have resulted in determinations of attractive and/or repulsive portions of the excited state potential energy curves which are accessible through transitions from the vibrationally cold ground electronic states. Concomitant observation of "hot" bands, or analysis of dispersed fluorescence, can provide analogous information about the ground state potential curves.

In our laboratories, we have recently been engaged in extensive spectroscopic characterizations of the ground-state and electronically excited triplet and singlet states of Cd·RG (RG = Ne, Ar, Kr, Xe) which are optically accessible.[12,16,20] These states correlate asymptotically with $Cd(5s5s\ ^1S_0)$, $Cd(5s5p\ ^3P_1)$, and $Cd(5s5p\ ^1P_1)$, respectively, and a ground-state Rg atom. There are several reasons for this. First of all, cadmium is a typical group II atom for which both triplet and singlet states can be accessed easily in convenient spectral regions, and can thus serve as a prototype for understanding van der Waals bonding of valence s^2 or sp metal atom electronic configurations with inert gas atoms of varying polarizability. Further, useful comparisons can be made with analogous spectroscopic information already available on the ground state and triplet excited states of Hg·Rg complexes.[6,10,17,18] Second, these potentials are important in understanding collisional electronic energy transfer processes observed previously in this laboratory.[1–5] Finally, Cd·Rg attractive potential curves should serve as approximations for the long-range forces felt by *molecules* interacting with $Cd(5s5p\ ^3P_1)$ or $Cd(5s5p\ ^1P_1)$. This could not only be important in understanding the mechanisms of the chemical or physical quenching processes of these states (which have been extensively studied in our laboratories),[1–4,23] but will also be useful in interpreting analogous half-collision experiments in which molecular van der Waals complexes of metal atoms are excited by tunable laser pulses.

In this paper, we report spectroscopic studies of the $X(^1\Sigma^+)$ ground states and the $A(^3\Sigma^+)$ triplet states [which correlate with $Cd(^3P_1) + Rg$] for CdNe, CdAr, CdKr, and CdXe. Characterization of the potential curves was accomplished by means of detailed analyses of rotational structure of high resolution LIF spectra of these species, as well as by analyses of dispersed fluorescence spectra for the CdAr transition. These results, when combined with those reported from earlier studies in our laboratories,[12,16,20] constitute a rather detailed picture of "sigma" and "pi" van der Waals bonding in the $X\ ^1\Sigma_{0^+}$, $A\ ^3\Sigma^+$, $B\ ^3\Pi_1$, $C\ ^1\Pi_1$, and $D\ ^1\Sigma_{0^+}$ states of CdNe, CdAr, CdKr, and CdXe.

EXPERIMENTAL

The supersonic beam apparatus has been described previously in Ref. 16 and recent modifications are dealt with in Ref. 20. Low resolution fluorescence excitation spectra and dispersed fluorescence spectra were obtained by excitation with frequency doubled laser pulses from a Molectron DL-16 dye laser pumped by the third harmonic of a Molectron MY-32 Nd:YAG laser. High resolution excitation spectra were obtained by excitation with the frequency doubled output of a Lumonics Hyperdye-300 dye laser pumped by XeCl (308 nm) excimer laser pulses (Lumonics Hyperex-400). A linewidth of about 0.002 nm is achieved with the Hyperdye laser, which utilizes a grazing incidence resonator. When a

[a] Present address: Science Institute, University of Iceland, Dunhaga 3, IS-107 Reykjavik, Iceland.
[b] Present address: Institute of Physics, University of Gdańsk, PL 80-952 Gdańsk, Poland.

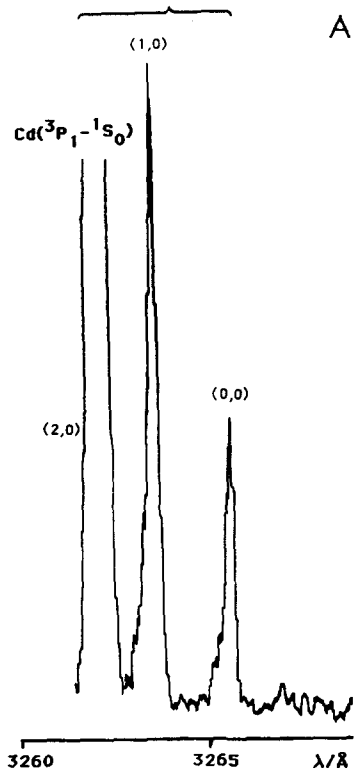

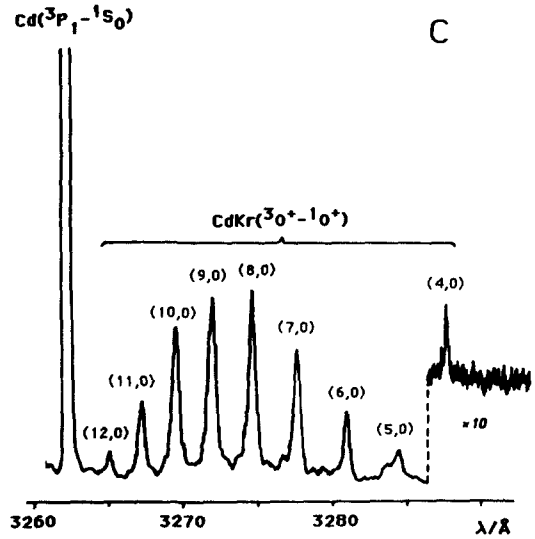

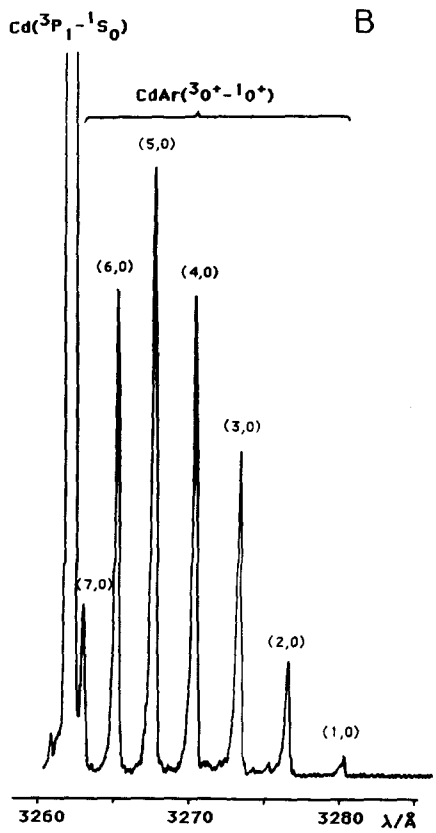

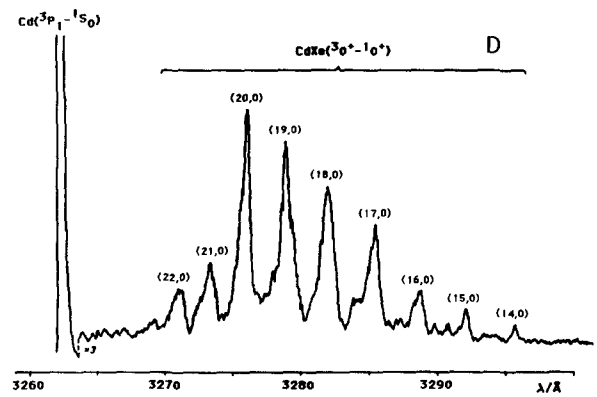

FIG. 1. Low resolution fluorescence excitation spectra of CdRg $A(^3O^+) \leftarrow X(^1O^+)$ transitions; Rg: (a) Ne; (b) Ar; (c) Kr; and (d) Xe. Assignment of bands is based on the analyses described in the text. The assignments for CdXe are uncertain by ± 1.

KD*P crystal is used for frequency doubling, this corresponds to a linewidth of about 0.08 cm^{-1} near the 326.2 nm transition of atomic cadmium, $Cd(5s5s\ ^1S_0) \rightarrow Cd(5s5p\ ^3P_1)$. The crystal was angle tuned for optimum phase matching with a homemade autotracking device when recording low resolution excitation spectra. The doubled radiation was separated from the fundamental by a Pellin–Broca prism and directed into the vacuum cell. The laser beam crossed the free jet expansion at 6–10 mm downstream from the nozzle (diameters 150–250 μm). Excitation spectra were obtained by placing a wide-band interference filter in front of an EMI 9816 QB photomultiplier tube situated at right angles to both the optical and supersonic jet axes. Dispersed fluorescence spectra were obtained by focusing the emitted radiation into a 1/2 m Jarrel–Ash monochromator, with detection by a Hamamatsu R212UH photomultiplier tube. The signals were processed with a PAR 164/165 boxcar integrator and recorded on an X–Y recorder.

Rare gases or rare gas mixtures were passed over cadmium metal heated in an oven to about 800 K (10 Torr cadmium vapor). Total backing pressure ranged from 4–12 atm. After expansion through the nozzle, rotational temperatures of 3–6 K were estimated from analyses of excitation spectra for CdNe and CdAr, as described below. High resolution excitation spectra of CdKr and CdXe were obtained by mixing $\approx 5\%$ Kr or 1% Xe with Ar, while those for CdNe and CdAr and all low resolution spectra were obtained by expanding with only the reagents of interest.

RESULTS AND ANALYSIS

Figure 1 shows low resolution fluorescence excitation spectra for the CdRg (Rg = Ne, Ar, Kr, Xe) $A(^3\!0^+) \leftarrow X(^1\!0^+)$ transitions. Previous analyses of the A–X spectra for CdNe, CdAr, and CdKr were based on the assumption that the bands observed at longest wavelength corresponded to the (0–0) transition.[16] Birge–Sponer plots based on the positions of bandheads thus resulted in lower limits for the vibrational frequencies (ω_e', ω_0') and bond strengths (D_e', D_0') for the $A(^3\!0^+)$ states, and approximate values for the anharmonicity constants $(\omega_e x_e', \omega_0 x_0')$. The current band assignments shown in Fig. 1 are based on analyses of the rotational structure of high resolution excitation spectra for CdRg (Rg = Ne, Ar, Kr, Xe), and dispersed fluorescence spectra for CdAr, which have resulted in verification of the previous assignment for CdNe and in reassignment of bands for the CdAr and CdKr spectra. All the bands are shaded to the blue, implying that the equilibrium bond lengths of the A states are shorter than those of the ground states.

High resolution fluorescence excitation spectra for the CdRg (A–X) transitions are shown in Figs. 2–6. As expected, only P and R branches are observed, clearly seen in Fig. 2 for CdNe, where the P-branch lines form bandheads but the R-branch lines dominate the structure to shorter wavelength. The spectra also display vibrational isotopic splittings. There are six cadmium isotopes of significant natural abundance (> 2%) and the number of significant isotopes of the rare gases are one, two, five, and six for Ar, Ne, Kr, and Xe, respectively. The number of isotopic combinations

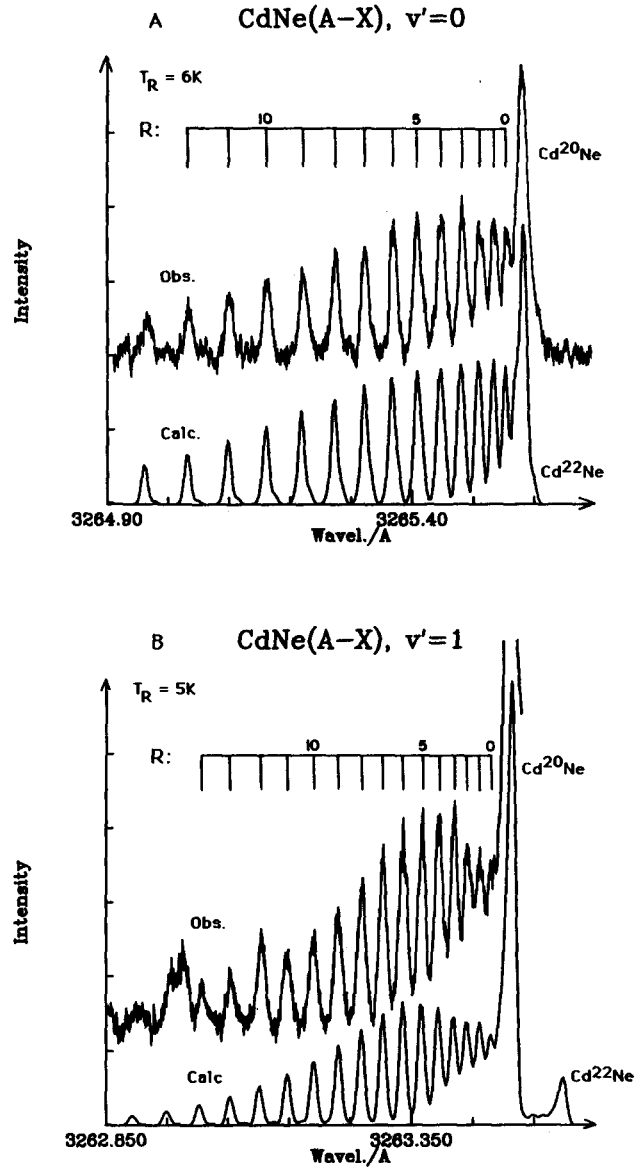

FIG. 2. Observed and best-fit high resolution excitation spectra for the CdNe $A(^3\!0^+) \leftarrow X(^1\!0^+)$ transitions, $v' = 0$ and 1. Spectroscopic constants are listed in Tables I and II. R-branch lines are indicated for $Cd^{20}Ne$ isotopic species.

therefore increases as CdAr(6) < CdNe(12) < CdKr(30) < CdXe(36). Isotopic splitting between two isotopic species (i and j) changes with masses and v' (for the A states) as[24]

$$\Delta(v',i,j) = (\rho_j - \rho_i)\omega_e'(v' + 1/2) - (\rho_j^2 - \rho_i^2)\omega_e x_e'(v' + 1/2)^2 + \delta + \Delta_f, \quad (1)$$

where $\rho_i^2 = \langle\mu\rangle/\mu_i$; $\langle\mu\rangle$ is the mean reduced mass based on the natural isotopic abundances, μ_i is the reduced mass of isotopic species i, δ is the contribution to the isotopic splitting by the $v'' = 0$ level of the ground electronic state, and Δ_f is the field shift due to the nuclear volume isotope effect in Cd. No nuclear magnetic hyperfine splitting is observed for this $0^+ \rightarrow 0^+$ electronic transition.[18] From Eq. (1), the isotopic splitting increases with v' to a maximum value of

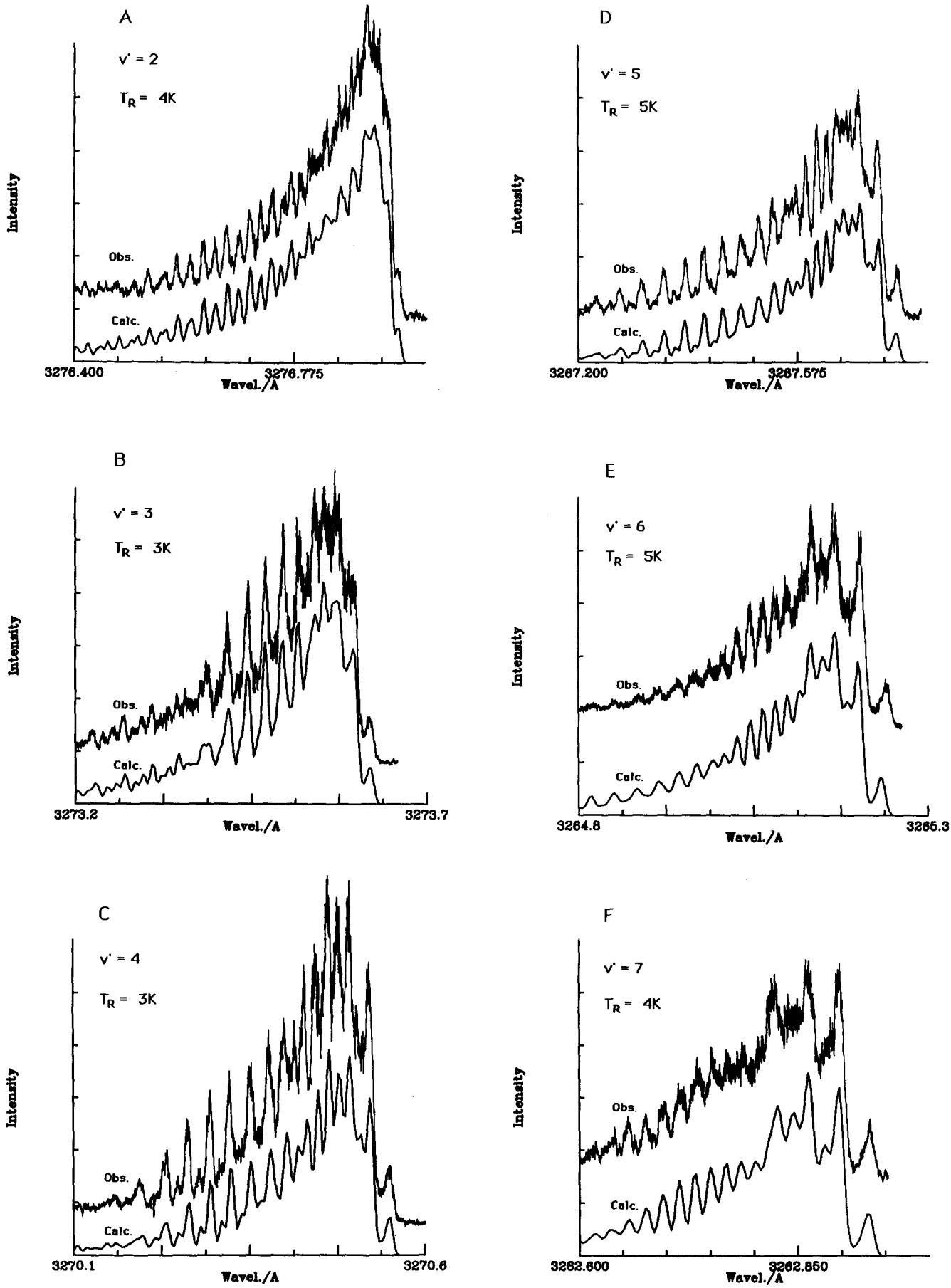

FIG. 3. Observed and best-fit high resolution excitation spectra for the CdAr $A(^3O^+) \leftarrow X(^1O^+)$ transitions, $v' = 2$–7. Spectroscopic constants are listed in Tables I and II.

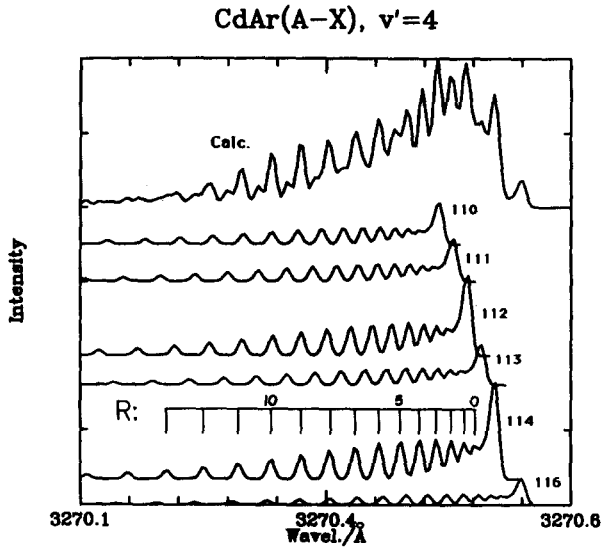

FIG. 4. Calculated contributions of isotopic species and total excitation spectrum for CdAr (A–X), $v' = 4$ transition. Isotopic contributions are marked by the atomic weights of Cd. R-branch lines for ^{114}CdAr are indicated.

$$v' \approx [(\rho_j - \rho_i)\omega_e'/2(\rho_j^2 - \rho_i^2)\omega_e x_e'] - 1/2 \qquad (2)$$

and then *decreases* at higher v'. (See Fig. 10.) Isotopic splitting for CdNe (low v' of 0 and 1) between isotopic combinations corresponding to different Cd isotopes but the same Ne isotope is found to be very small and unmeasurable with our resolution (Fig. 2). For the other CdRg states (Rg = Ar, Kr, Xe), where v' is greater, isotopic splitting is relatively large, and the spectra consist of contributions due to different isotopic species which are very similar in rotational structure but shifted relative to one another with spectral line intensities determined by the natural isotopic abundances, as can be seen in Fig. 4 for CdAr. Bandheads of the most significant isotopic contributions are marked on Figs. 2 and 4–6.

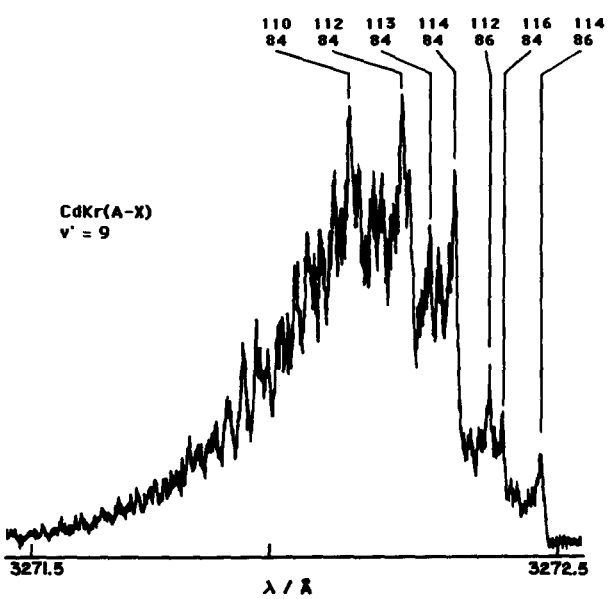

FIG. 5. Observed high resolution excitation spectrum for CdKr (A–X), $v' = 9$ transition. Bandheads of main isotopic contributions are marked by atomic weights of Cd (upper numbers) and Kr (lower numbers) isotopes.

Anharmonicity constants ($\omega_e x_e'$) for the A states of CdRg (Rg = Ar, Kr, Xe) were reevaluated from Birge–Sponer-like analyses of isotopic bandheads based on

$$\Delta\nu_{v'}(i) = \nu_{v'+1}(i) - \nu_{v'}(i)$$
$$= \rho_i\omega_e' - 2\cdot\rho_i^2\omega_e x_e'\{v'+1\}, \qquad (3)$$

where $\nu_{v'}(i)$ and $\nu_{v'+1}(i)$ are the positions of the bandheads for isotopic species (i) for vibrational levels v' and $v'+1$, respectively. The $\omega_e x_e'$ values were obtained either from slopes of plots of $\Delta\nu(i)$ vs $v'+1$ (for CdAr) or as a solution of two equations of type (3):

$$\omega_e x_e' = (\Delta\nu_{v'} - \Delta\nu_{v'+1})/2\cdot\rho_i^2 \qquad (4)$$

for CdKr and CdXe. Results are listed in Table I.

Assignments of vibrational bandheads (v') for CdRg (Rg = Ne, Ar, Kr, Xe) were made from analyses of isotopic bandheads and splittings in the following way: Positions of isotopic bandheads were approximated by the expression

$$\nu_i = T_e' + \rho_i\omega_e'(v'+1/2) - \rho_i^2\omega_e x_e'(v'+1/2)$$
$$- \rho_i\omega_e''(1/2) + \rho_i^2\omega_e x_e''(1/4). \qquad (5)$$

Using $\omega_e x_e'$ in Table I and ω_e'' and $\omega_e x_e''$ from Ref. 20, approximate values for T_e' and ω_e' were obtained by solving Eq. (5) for two isotopic bandheads of the same v' level. This was done for several v' levels for an assumed assignment. The procedure was repeated for different assignments, and a search was made for the assignment which gave the most consistent T_e' and ω_e' values for all v' levels (see CdKr and CdXe analyses below).

CdNe and CdAr

High resolution fluorescence spectra for CdNe and CdAr, shown in Figs. 2 and 3, were computer simulated. Isotopic splittings due to nuclear field shifts for Cd isotopes are very low,[25,26] and good fits could be obtained by disregarding these and assuming the splitting to be dominantly vibrational. The values for $B_{v'}$ and the rotational temperature (T_R) were allowed to vary for each v' band in the simulations, while consistent values for ω_e', $B_{v'=0}$ and T_e' independent of v', were sought. B_e' and α_e' for the upper states were evaluated from the functional relationship between B_v and v[24]:

$$B_v = B_e + \alpha_e(v + 1/2) \qquad (6)$$

and r_e' was determined. B_e'' (and r_e'') for the ground state were estimated from Eq. (6) for $v'' = 0$ by using a calculated α_e''[24]:

$$\alpha_e'' = [6\cdot(\omega_e x_e''\cdot B_e''^3)^{1/2}/w_e''] - [6\cdot B_e''^2/\omega_e''] \qquad (7)$$

and ω_e'' and $\omega_e x_e''$ values from Ref. 20.

Having determined r_e' and r_e'', Franck–Condon factors for the A–X transitions were calculated and compared with the excitation spectra to further verify the consistency of the v' assignments. Morse potential expressions were assumed for the A states and potential curves from Ref. 20 were used for the X states.

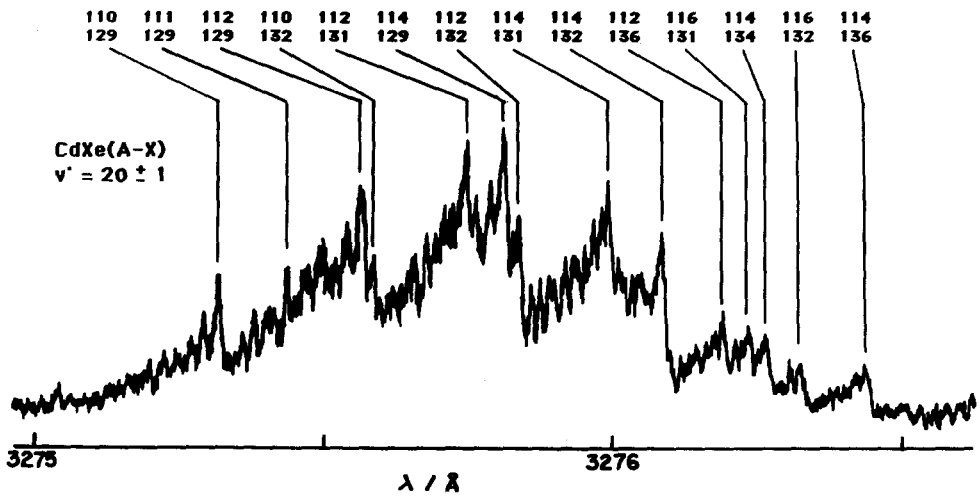

FIG. 6. Observed high resolution excitation spectrum for CdXe (A–X), $v' = 20 \pm 1$ transition. Bandheads of main isotopic contributions are marked with atomic weights of Cd (upper numbers) and Xe (lower numbers) isotopes.

CdNe

The assignment of the vibrational bands was found to be consistent with the previous one.[16] The band observed at the longest wavelength is due to the (0–0) transition [Figs. 1(a) and 2(a)]. The irregularity in the rotational structure for the (1–0) band near 326.3 nm [Fig. 2(b)] is believed to be due to CdXe, since slight Xe contamination of the Ne gas was discovered at a later date. The almost exact superposition of contributions from isotopic combinations corresponding to different Cd isotopes (with the same Ne isotope) allows estimates of $\{B'_{v'} - B''_{v''=0}\}$ from spacings between R-branch lines:

$$\Delta\nu_J = \nu_{J+1} - \nu_J = 2\{B' - B''\}J + 2\{2B' - B''\}. \quad (8)$$

The $\{B' - B''\}$ values were obtained from the slopes of plots of $\Delta\nu_J$ against J (Fig. 7). Furthermore, B' and B'' could be estimated for an assumed J assignment of lines from intercept values as well as the slopes. These served as starting values for the simulations, which resulted in best fits of experimental and calculated spectra (Fig. 2) for the J assignments shown in Figs. 2 and 7. Rotational constants, ω'_e, and T'_e are listed in Tables I and II. The $\omega_e x'_e$ value used is from an earlier determination.[16] The equilibrium internuclear distances are 4.26 ± 0.05 and 3.62 ± 0.05 Å for the X and the A states, respectively. It is noteworthy that the spectra could easily be simulated without making use of D_v (D_e) constants. Positions of R-branch lines depend on $(D_{v''=0'} - D_{v'})$ to a first approximation ($D_v \ll B_v$) as

TABLE I. Spectroscopic constants for CdRg (Rg = Ne, Ar, Kr, Xe). Constants listed are for CdRg molecules with the mean isotopic abundance compositions of Cd and Rg atoms.

		CdNe	CdAr	CdKr	CdXe
$A(^3\Omega^+)$	ω'_e(cm^{-1})	22.6	38.5	37.1	50.7
State	$\omega_e x'_e$(cm^{-1})	1.6[a]	1.22	0.65	0.6
	α'_e[b](cm^{-1})	0.0075	0.0017		
	B'_e[b](cm^{-1})	0.0753	0.0481		
	r'_e(Å)	3.62 ± 0.05	3.45 ± 0.03		
	T'_e[c](cm^{-1})	30 619	30 437	30 274	$29\,746 \pm 40$
	D'_e[d](cm^{-1})	77	325	513	$1\,086 \pm 40$
	D'[e](cm^{-1})	80	304	529	1 071
	C_{12}[f](cm^{-1} Å^{12})	5.380×10^8	2.047×10^9		
	C_6[f](cm^{-1} Å^6)	3.991×10^5	1.385×10^6		
$X(^1\Omega^+)$	B''_e(cm^{-1})	0.0542	0.0306		
State	r''_e(Å)	4.26 ± 0.05	4.33 ± 0.04		

[a]From Ref. 16.
[b]From Eq. (6) and data in Table II.
[c]Based on $T''_e = 0$ [for the $X(^1\Omega^+)$ states].
[d]$d'_e = E(^3P_1) + D_e(X\text{-state}) - T'_e$; $D_e(X)$ from Refs. 16 and 20.
[e]$D' = \omega_e'^2/4\,\omega_e x'_e$ (Morse potential extrapolation).
[f]Parameters in Lennard-Jones potentials used to express A state potential curves at long range; $r > 4.37$ Å for CdNe and $r > 4.75$ Å for CdAr.

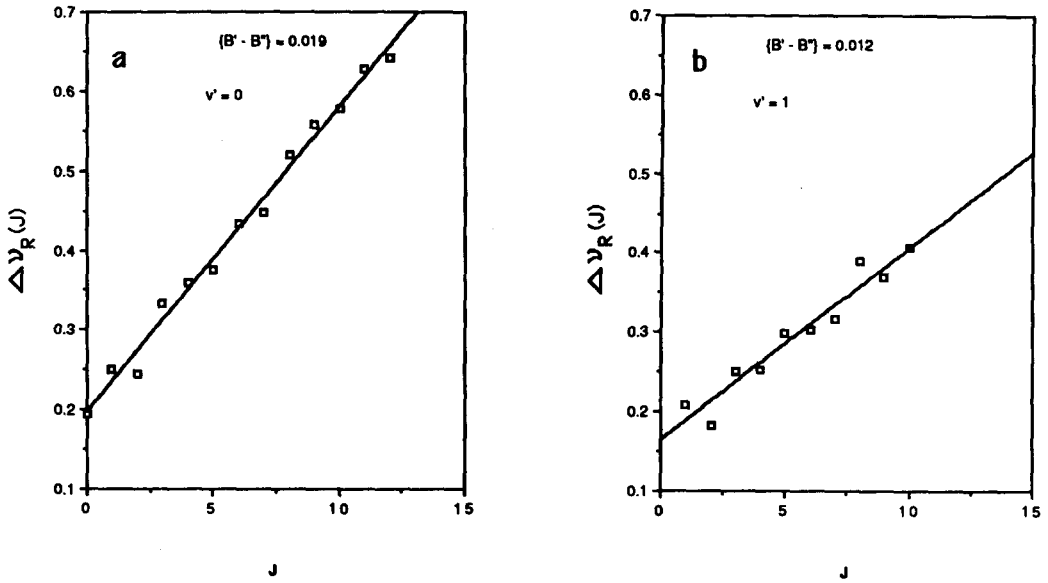

FIG. 7. Spacing between R-branch lines (plotted against J) in CdNe (A–X) transition excitation spectra for (a) $v'=0$ and (b) $v'=1$ (see Fig. 2).

$$\nu_r \approx \nu_{v'}^0 + \{B' - B''\}J^2 + \{3B' - B''\}J + 2B' + 2\{D'' - 3D'\}J^3 + \{D'' - D'\}J^4. \quad (9)$$

The D_v constants could be estimated from B_e, α_e, ω_e, and $\omega_e x_e$ as described in Ref. 24 (pp. 107–108). Thus $D_{v'=0} = 3.3\times10^{-6}$ cm^{-1}, $D_{v'=1} = 3.1\times10^{-6}$ cm^{-1}, and $D_{v''=0} = 3.4\times10^{-6}$ cm^{-1} were obtained. The last two terms in Eq. (9) were found to be negligible for observed $J(J<14)$ and insignificant changes in the position of rotational lines were observed when including D_v values in the simulations.

Franck–Condon factor calculations [Fig. 8(a)] show good agreement with the observations for $v'=0$ and 1 bands [Fig. 1(a)] and suggest that a relatively strong band due to the (2–0) transition is overlapping the cadmium atomic line, as suggested before.[16]

CdAr

In addition to determining the v' assignment from isotopic splittings, a confirmation of the assignment could be made from dispersed fluorescence spectra for transitions from individual upper state vibrational levels.[20] Such transitions give spectra with oscillatory structure, where the number of minima correspond to the number of nodes (= vibrational quantum number) in the upper state vibrational wave

TABLE II. Rotational constants and interatomic distances of CdNe and CdAr for the A and X states. Constants listed are for CdNe and CdAr molecules with the mean isotopic abundances for each atom.

		v	B_v(cm^{-1})	r_v(Å)
CdNe	$X(^1\Sigma^+)$	0	0.0518	4.36
	$A(^3\Sigma^+)$	0	0.0716	3.71
		1	0.0642	3.92
CdAr	$X(^1\Sigma^+)$	0	0.0302	4.35
	$A(^3\Sigma^+)$	2	0.0440	3.61
		3	0.0422	3.68
		4	0.0406	3.75
		5	0.0390	3.83
		6	0.0372	3.92
		7	0.0356	4.01

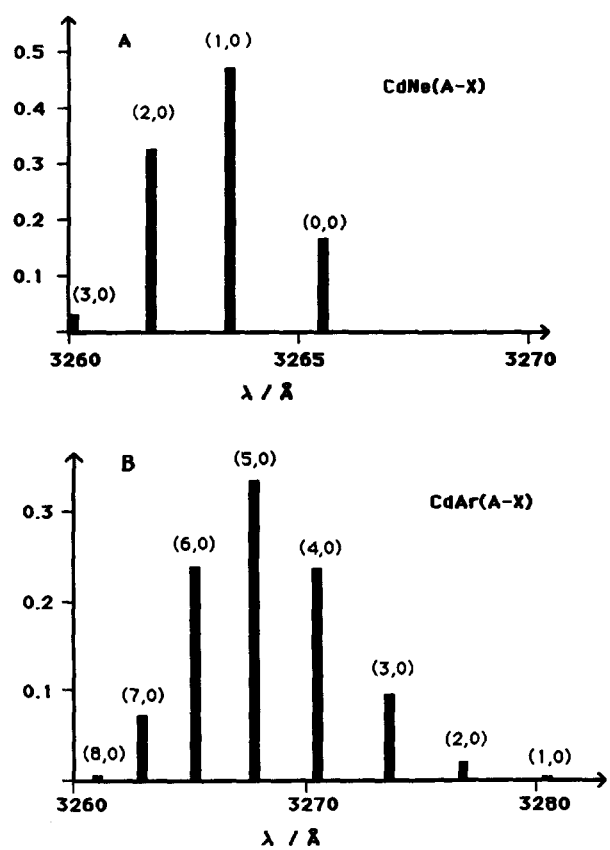

FIG. 8. Calculated Franck–Condon factors for the A–X transitions for CdNe and CdAr. Morse potentials are assumed for the A states, and the potentials of the X states are expressed as sums of repulsive exponential terms and attractive C_6 terms (see the text).

functions. However, due to the long radiative lifetime of the A state[16] [$\tau(^3O^+) = 2.4 + 0.2\ \mu s$] the excited state species experience a few collisions with background Ar gas in the jet before fluorescing, and thus undergo vibrational relaxation. The dispersed fluorescence spectra at long delay times therefore consist of overlapping vibrational contributions, so that the true oscillatory structure may be lost, as shown in Fig. 9(a). This depends on the boxcar integrator sampling time, however. By shortening the sampling time to 500 ns, oscillations were indeed observed, since there is less contribution from lower vibrational levels formed by collisional deactivation [Fig. 9(b)]. The bandhead at 327.36 nm was therefore assigned to the (3–0) transition. Vibrational quantum number assignments are therefore one higher than previously assumed.[16]

The high resolution excitation spectra for CdAr ($v = 2$–7; Fig. 3) show more irregular structure than the CdNe spectra because of greater isotopic splitting due to the Cd isotopes. The P-branch bandheads of individual isotopic contributions form the longest wavelength peaks and shoulders of each vibrational spectrum, clearly separated for $v' > 3$. Simulations of spectra are shown in Figs. 3 and 4 and spectroscopic constants are listed in Tables I and II. A plot of $B_{v'}$ against v' exhibits a straight line, allowing determination of α_e', B_e', and r_e' [Eq. (6)]. The internuclear distances are thus 4.33 ± 0.04 and 3.45 ± 0.03 Å for the X and the A states, respectively. The isotopic shift calculated from Eq. (1) increases and reaches a maximum value at $v' = 7$–8 [Eq. (2), Fig. 10(a)]. Analogous to the CdNe simulations, no need was found to include the rotational constants D_v (D_e). Esti-

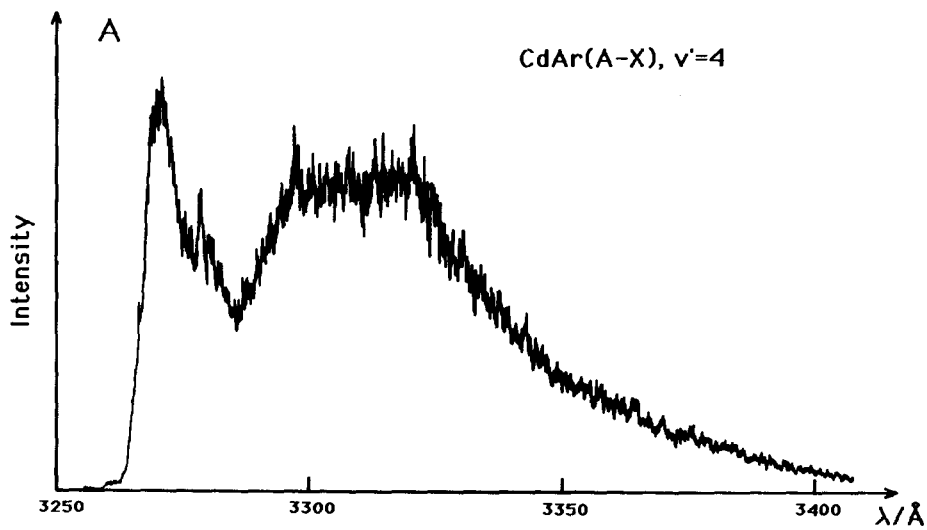

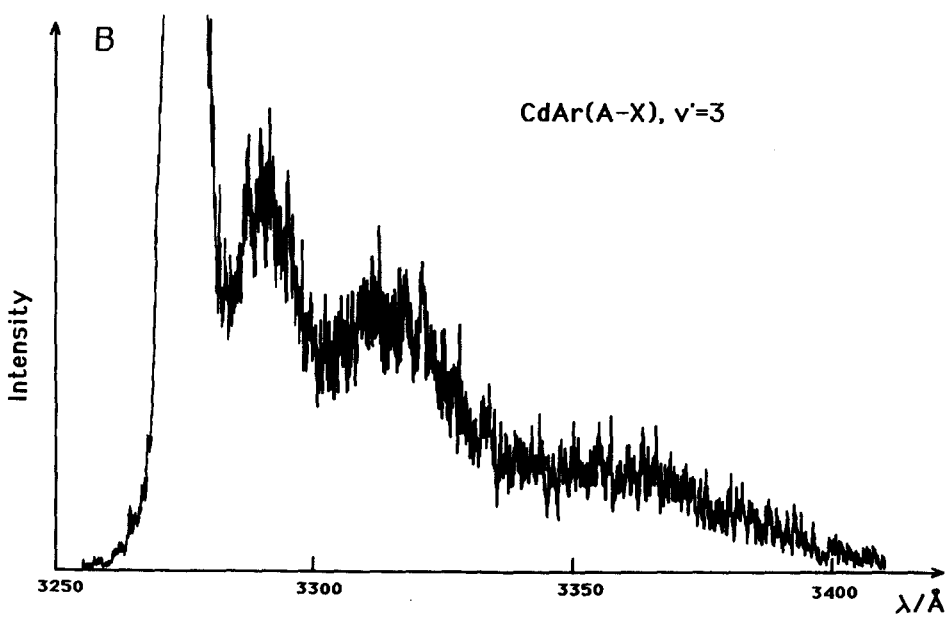

FIG. 9. Dispersed fluorescence spectra for CdAr (A–X) transitions for (a) 2 μs ($v' = 4$) and (b) 500 ns ($v' = 3$) boxcar integrator sampling times.

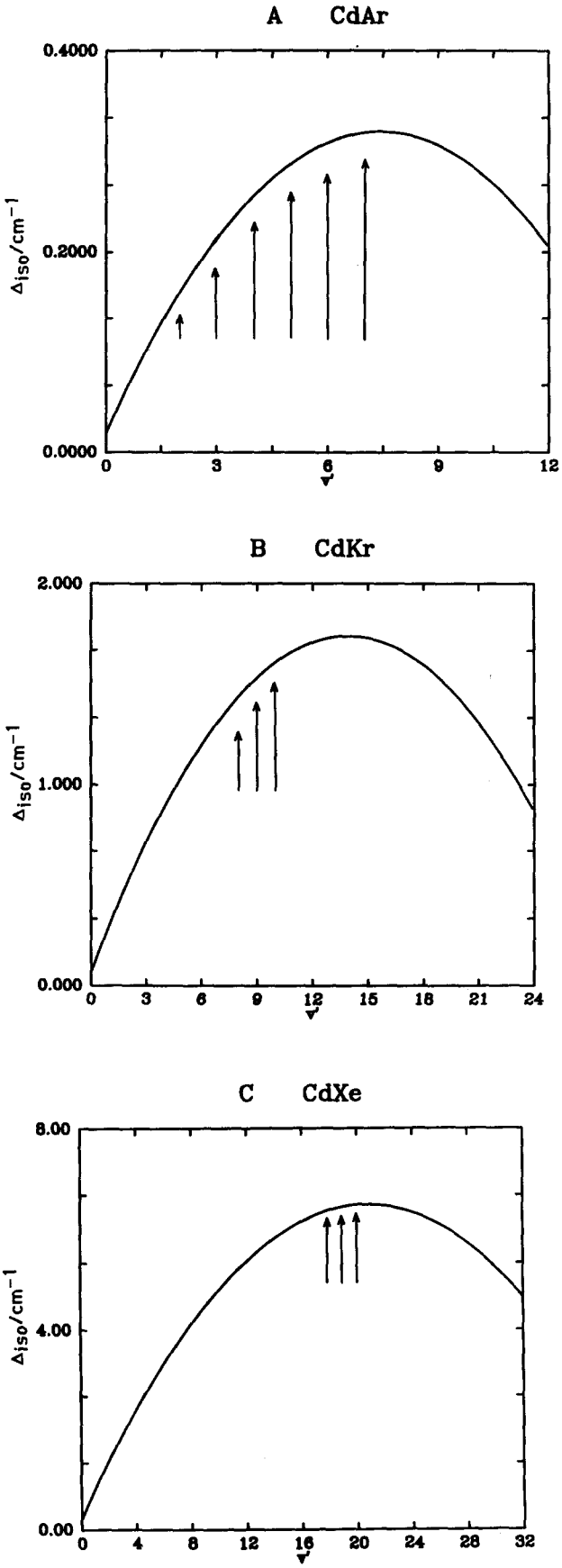

FIG. 10. Isotopic splittings. Solid lines are according to Eq. (1). Arrows indicate isotopic shifts for vibrational levels used in the analyses of high resolution spectra and assignments of vibrational bands (see the text). (a) For ^{116}CdAr and ^{114}CdAr isotopic species. (b) For $^{114}Cd^{86}Kr$ and $^{114}Cd^{84}Kr$ species. (c) For $^{114}Cd^{136}Xe$ and $^{114}Cd^{129}Xe$ species.

mated values of $D_{v'}$'s ranged from 3.3×10^{-7} to 3.8×10^{-7} cm^{-1} for $v'=2$–7 while $D_{v'=0}$ is about 2.9×10^{-7}. The contribution of the last term in Eq. (9) for observed lines ($J<15$) was again found to be negligible.

Franck–Condon factor calculations [Fig. 8(b)] show very good agreement with experimental observations [Fig. 1(b)], indicating that a correct assignment of vibrational bandheads has been made, and that the difference in average internuclear distances for the X and the A states is correctly determined.

CdKr

The assignment of vibrational bands in the A–X excitation spectrum for CdKr was made by comparing positions of bandheads of two isotopic species such as $^{114}Cd^{86}Kr$ and $^{114}Cd^{84}Kr$ (Fig. 5) for three different v' levels, as described previously. As a measure of the consistency of ω'_e and T'_e values obtained from the three vibrational bands (326.95, 327.22, and 327.46 nm), the standard deviations (σ) were evaluated and plotted against the lowest vibrational level quantum number [v'_{min}; Fig. 11(a)] for different possible assignments. The minima in these plots are found for a (consistent) value of $v'_{min}=8$, which therefore is the v' assignment for the 327.46 nm vibrational band in the excitation spectrum, four quanta higher than an earlier estimate.[16] The ω'_e and $\omega_e x'_e$ values obtained from Birge–Sponer-like analyses (see above) of isotopic bandheads are listed in Table I, along with T'_e.

CdXe

Three high resolution vibrational bands were analyzed in a similar fashion as described for CdKr, using two isotopic bandheads (Fig. 6). Since ω''_e and $\omega_e x''_e$ for ground state CdXe are unknown, so are the last two terms in Eq. (5). The effect of using different ω''_e and $\omega_e x''_e$ values (within realistic ranges), however, turned out not to affect the assignment determination. Typical standard deviation values (vs v_{min}) for the isotope species $^{114}Cd^{136}Xe$ and $^{114}Cd^{129}Xe$ are shown in Fig. 11(b). Thus an assignment of $v'=18\pm1$ for the 328.17 nm band was obtained. The greater uncertainty in the assignment for CdXe than for CdKr (and CdAr) is mostly due to the fact that the v' bandheads observable for CdXe are for very high v' levels, where the isotopic splitting happens to vary slowly with v', while those for CdKr (and CdAr) correspond to lower v' levels where the slope of isotopic splitting vs v' is greater (see Fig. 10). The ω'_e,$\omega_e x'_e$, and T'_e values are listed in Table I.

POTENTIAL CURVES

Vibrational frequencies and anharmonicity constants for the A states (Table I) are based on Birge–Sponer-like analyses, and the potential curves can be expressed as Morse potentials:

$$V_A(r)=T'_e+D'\{1-\exp[-\beta(r-r'_e)]\}^2,$$
$$\beta=0.121\,778\omega_e(\langle\mu\rangle/D_e)^{1/2}. \quad (12)$$

Since the Birge–Sponer plots exhibit near linear behavior,[16] these potentials are valid for vibrational levels less than or

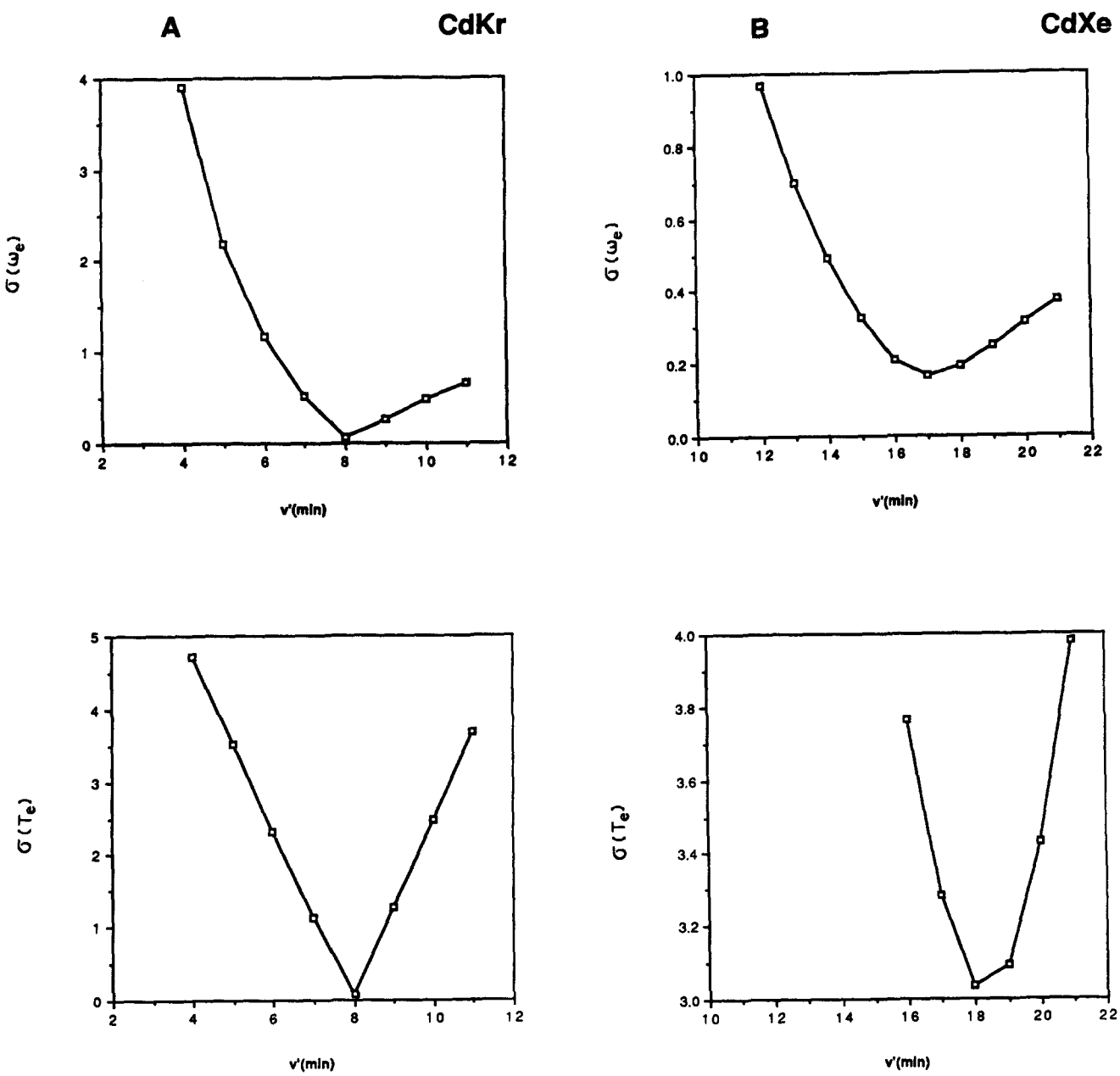

FIG. 11. Standard deviation of T'_e and ω'_e values (cm^{-1}) evaluated from Eq. (5) for three vibrational bands for (a) CdKr; isotopic species $^{114}Cd^{86}Kr$ and $^{114}Cd^{84}Kr$ and (b) CdXe; isotopic species $^{114}Cd^{136}Xe$ and $^{114}Cd^{129}Xe$ (see the text).

equal to the highest v' observed (Fig. 1). Such curves, however, show slight deviations from the asymptotic limit, $Cd(^3P_1) + Rg(^1S)$, as revealed by comparing D' $(= \omega_e'^2/4\omega_e x'_e)$ in the Morse potential expression with D'_e based on our experimental results $[D'_e = E(^3P_1) + D''_e(X) - T'_e)]$ (Table I). To correct for this, we switched to a Lennard-Jones-type C_6/C_{12} potential at larger r, which controlled the slope of the potential at internuclear distances just outside those accessible from the $v'' = 0$ ground state (Table I).

Analyses of the shape of the ground state potentials for CdNe and CdAr were done earlier in this laboratory from dispersed fluorescence spectra for the $C(^1\Pi_1) \leftarrow X(^1 0^+)$ transitions.[20] The internuclear distances determined here (Table I) were utilized in Ref. 20, where the ground state potentials were expressed as repulsive exponential terms plus attractive C_6 terms.

DISCUSSION

Bond energies for the $A(^3 0^+)$ states of MRg (M = Cd, Hg and Rg = Ne, Ar, Kr, and Xe) obtained from LIF experiments, line broadening experiments and pseudopotential calculations are summarized in Table III. Changes in assignments of vibrational bands from those reported ear-

TABLE III. Dissociation energies for CdRg and HgRg $A(^3O^+)$ states. Superscript numbers inside parentheses are reference numbers.

	D_e (cm^{-1})						
	Cd			Hg			
				LIF studies (Ref. 18)			
	This work (LIF)[a]	LIF studies (Ref. 16)[b]	Pseudopot. calc.	a	b	Line broadening	Pseudopot. calc.
Ne	77	⩾75	26.3[27]	83	108[c]		33[27]
Ar	325	⩾282	326[28]	376	369	430[32]	
Kr	513	⩾373	407[28]		>517		
Xe	1086		360[28]		1457	1400[31], 1450[33]	

[a]From rotational structure analyses.
[b]From low resolution excitation spectra.
[c]Corrected value, see Ref. 16.

lier[16] for CdAr and CdKr resulted in larger values for ω_e' and therefore higher bond energies, D_e'. The earlier estimate of D_e' for CdNe was confirmed, however. No information on the CdRg ($A\,^3O^+$) state potentials are available from line broadening experiments. Czuchaj *et al.*[27] performed pseudopotential SCF/CI calculations for the potential energies of CdNe and HgNe, A and X states. The bond energies obtained are lower than the experimentally determined values, both for CdNe and HgNe (Table III), which may be due to the quality of the pseudopotentials used for Ne. Czuchaj and Sienkiewicz also performed semiempirical pseudopotential calculations for CdRg (Rg = Ar, Kr, and Xe),[28] based on the method of Baylis.[29] While the bond energies calculated for CdKr and CdXe A states are badly underestimated, the value for CdAr $A(^3O^+)$ is very similar to that obtained spectroscopically (which may, however, be fortuitous).

The experimental results indicate that dissociation energies for CdRg(A) [and HgRg(A)] increase with the atomic number of the rare gas. This is undoubtedly due to increasing polarizability[30] and greater long range attractive forces in the order Ne < Ar < Kr < Xe. The C_6 parameter in the attractive term of the Lennard-Jones potential we used to represent the CdAr A state, at long range is, in fact, larger than for CdNe, although it should be recognized that these values were obtained only to permit smooth dissociation to the correct asymptotes and are not meant to represent quantitative C_6 values. D_e's for CdRg(A) are generally found to be lower than the corresponding values for HgRg(A), as is also found to be the case for the ground states.[12,17,18,20] This could be due to a greater effective polarizability of the mercury vs the cadmium atomic states.

The available values for equilibrium internuclear distances for the $A(^3O^+)$ and the $X(^1O^+)$ states of CdRg and HgRg are summarized in Table IV. The only experimental values for CdRg are those presented in this paper. The r_e value for the X state of CdAr is found to be slighly greater than that for CdNe, analogous to what is found for the ground state of HgNe and HgAr. The r_e value for the A state of CdAr, on the other hand, is found to be slightly less than that for CdNe, as also found for HgNe and HgAr from rotational structure analyses.[18] Equilibrium internuclear distances, both for the A and the X states, are greater for CdNe

TABLE IV. Equilibrium internuclear distances for CdRg and HgRg $X(^1O^+)$ and $A(^3O^+)$ states. Superscript numbers are reference numbers.

		r_e (Å)							
		Cd			Hg				
					LIF studies (Ref. 18)				
		This work (LIF)[a]	Pseudopot. calc.	Mixing rules (Ref. 28)	a	b	Line broadening	Photoionization studies[35]	Pseudopot. calc.[27]
$A(^3O^+)$	Ne	3.62	4.34[27]		3.47	3.12			3.65
	Ar	3.45	3.39[28]		3.36	3.38			
	Kr		3.44[28]			3.52			
	Xe		3.78[28]			3.25	3[33]		
$X(^1O^+)$	Ne	4.26	5.24[27]		3.90	3.87			4.65
	Ar	4.33	3.49[28]	3.49	3.99	4.01			
	Kr		3.55[28]	3.64		4.07	3.95[34]	3.98	
	Xe		3.73[28]	3.80		4.25	4.10[33]	4.23	

[a]Rotational structure analyses.
[b]Estimates from FC factor calculations.

and CdAr than for HgNe and HgAr, respectively. This is consistent with the fact that the diameter of the Cd atom is slightly greater than the Hg atom.[1]

The r_e's for CdNe and HgNe, A and X states, obtained from pseudopotential calculations are higher than the experimental values, probably due to an overestimate of the repulsive forces in the calculations.[27] On the other hand, the calculated r_e values[28] for the CdAr A and X states are lower.

A comparison has been made between van der Waals bonding in the $A(^3O^+)$ and $C(^1\Pi_1)$ states of the CdRg molecules.[20] Both the $A(^3O^+)$ and $C(^1\Pi_1)$ states correspond to a pure "Π" orientation of the Cd p orbital. The $C(^1\Pi_1)$ states, which correlate with $Cd(^1P_1)$ + Rg, are found to be more deeply bound than the corresponding $A(^3O^+)$ states, which correlate with $Cd(^3P_1)$ + Rg. This has been attributed to a larger polarizability and less steep repulsive potential due to the larger spatial extent of the p orbital in the singlet vs the triplet state, and the more diffuse electron density associated with the p orbital in this state.[20]

ACKNOWLEDGMENTS

We are grateful to the National Science Foundation for the support of this research. One of us (A.K.) would like to thank the Fulbright program for a fellowship and the University of Utah for his appointment as a Visiting Associate Professor in Spring 1988.

[1]W. H. Breckenridge and H. Umemoto, in *The Dynamics of the Excited State*, edited by K. Lawley (Wiley, New York, 1982).
[2]W. H. Breckenridge and A. M. Renlund, J. Phys. Chem. **82**, 1474, 1484 (1978).
[3]W. H. Breckenridge and O. K. Malmin, J. Chem. Phys. **74**, 3307 (1981).
[4]W. H. Breckenridge, W. L. Nikolai, and D. Oba, J. Phys. Chem. **90**, 5724 (1986).
[5]W. H. Breckenridge and C. N. Merrow, J. Chem. Phys. **88**, 2320, 2329 (1988).
[6]W. H. Breckenridge, O. Benoist d'Azy, M. C. Duval, C. Jouvet, and B. Soep, in *Stochasticity and Intramolecular Redistribution of Energy*, edited by R. Lefebvre and S. Mukamel (Reidel, Dordrecht, 1987), p. 149, and references cited therein.
[7]W. J. Alford, N. Andersen, M. Belsley, J. Cooper, D. M. Warrington, and K. Burnett, Phys. Rev. A **31**, 3012 (1985), and references therein.
[8]W. Bussert, D. Neuschäfer, and S. R. Leone, J. Chem. Phys. **87**, 3833 (1987), and references therein.
[9]R. Düren and E. Hasselbrink, J. Chem. Phys. **85**, 1880 (1986), and references therein.
[10]W. H. Breckenridge, C. Jouvet, and B. Soep, J. Chem. Phys. **84**, 1443 (1986).
[11]M. C. Duval, B. Soep, R. D. van Zee, W. B. Bosma, and T. S. Zwier, J. Chem. Phys. **88**, 2148 (1988).
[12]D. J. Funk and W. H. Breckenridge (submitted).
[13]R. E. Smalley, D. A. Auerbach, P. S. H. Fitch, D. H. Levy, and L. Wharton, J. Chem. Phys. **66**, 3778 (1977); J. Tellinghuisen, A. Ragone, M. S. Kim, D. J. Auerbach, R. E. Smalley, L. Wharton, and D. H. Levy, *ibid.* **71**, 1283 (1979).
[14]W. P. Lapatovich, R. Ahmed-Bitar, P. E. Moskowitz, I. Renhorn, R. A. Gottscho, and D. E. Pritchard, J. Chem. Phys. **73**, 5419 (1980); R. A. Gottscho, R. Ahmed-Bitar, W. P. Lapatovich, I. Renhorn, and D. E. Pritchard, *ibid.* **75**, 2546 (1981).
[15]A. Kowalski, D. J. Funk, and W. H. Breckenridge, Chem. Phys. Lett. **132**, 263 (1986).
[16]A. Kowalski, M. Czajkowski, and W. H. Breckenridge, Chem. Phys. Lett. **121**, 217 (1985).
[17]M.-C. Duval O. Benoist d'Azy, W. H. Breckenridge, C. Jouvet, and B. Soep, J. Chem. Phys. **85**, 6324 (1986).
[18]K. Hamahouchi, S. Isagai, M. Okunishi, and S. Tsuchiya, J. Chem. Phys. **88**, 205 (1988); K. Yamanouchi, J. Fukuyama, H. Horiguchi, S. Tsuchiya, K. Fuke, T. Saito, and K. Kaya, *ibid.* **85**, 1806 (1986); K. Fuke, T. Saito, and K. Kaya, *ibid.* **81**, 2591 (1984).
[19]J. M. Gardner and M. I. Lester, Chem. Phys. Lett. **137**, 301 (1987).
[20]D. J. Funk, A. Kvaran, and W. H. Breckenridge (submitted).
[21]E. Zanger, V. Schmatloch, and D. Zimmerman, J. Chem. Phys. **88**, 5396 (1988).
[22]R. Bennett, J. G. McCaffrey, I. Wallace, D. J. Funk, A. Kowalski, and W. H. Breckenridge (submitted).
[23]W. H. Breckenridge, H. Umemoto, and J.-H. Wang, Chem. Phys. Lett. **123**, 23 (1986).
[24]G. Herzberg, *Molecular Spectra and Molecular Structure, I. Spectra of Diatomic Molecules* (Van Nostrand Reinholt, New York, 1950).
[25]R. J. Hull and H. H. Stroke, J. Opt. Soc. Am. **53**, 1147 (1963).
[26]P. Brix and A. Steudel, Z. Phys. **128**, 260 (1950).
[27]E. Czuchaj, H. Stoll, and H. Preuss, J. Phys. B **20**, 1487 (1987).
[28]E. Czuchaj and J. Sienkiewicz, J. Phys. B **17**, 2251 (1984).
[29]W. E. Baylis, J. Chem. Phys. **51**, 2665 (1969).
[30]C. Bousquet, J. Phys. B **19**, 3859 (1986).
[31]L. K. Lam, A. Gallagher, and R. Drullinger, J. Chem. Phys. **68**, 4411 (1978).
[32]C. Petzold and W. Behmenburg, Z. Naturforsch. Teil A **33**, 1461 (1978).
[33]T. Grycuk and M. Findeisen, J. Phys. B **16**, 975 (1983).
[34]J. Grycuk and E. Czerwosz, Physica C **106**, 431 (1981).
[35]C. L. Liao and C. Y. Ng, J. Chem. Phys. **84**, 1142 (1986).